

Electrochemical Impedance Spectroscopic Analysis of Dye-Sensitized Solar Cells

Qing Wang, Jacques-E. Moser, and Michael Grätzel*

Laboratory for Photonics and Interfaces, Institute of Chemical Sciences and Engineering, Ecole Polytechnique Fédérale de Lausanne, 1015 Lausanne, Switzerland

Received: May 25, 2005

Electrochemical impedance spectroscopy (EIS) has been performed to investigate electronic and ionic processes in dye-sensitized solar cells (DSC). A theoretical model has been elaborated, to interpret the frequency response of the device. The high-frequency feature is attributed to the charge transfer at the counter electrode while the response in the intermediate-frequency region is associated with the electron transport in the mesoscopic TiO₂ film and the back reaction at the TiO₂/electrolyte interface. The low-frequency region reflects the diffusion in the electrolyte. Using an appropriate equivalent circuit, the electron transport rate and electron lifetime in the mesoscopic film have been derived, which agree with the values derived from transient photocurrent and photovoltage measurements. The EIS measurements show that DSC performance variations under prolonged thermal aging result mainly from the decrease in the lifetime of the conduction band electron in the TiO₂ film.

1. Introduction

Dye-sensitized solar cells (DSC) present a promising alternative to conventional photovoltaic devices.^{1–4} After more than one decade's development, it has reached global AM 1.5 power conversion efficiencies up to 11%.⁵ At the heart of the DSC is a mesoscopic semiconductor oxide film typically made of TiO₂, whose surface is covered with a monolayer of sensitizer (Figure 1). During the illumination of the cell, electrons are injected from the photoexcited dye into the conduction band of the oxide. From there they pass through the nanoparticles to the transparent conducting oxide current collector into the external circuit. The sensitizer is regenerated by electron transfer from a donor, typically iodide ions, which are dissolved in the electrolyte that is present in the pores. The triiodide ions formed during the reaction diffuse to the counter electrode where they are reduced back to iodide by the conduction band electrons that have passed through the external circuit performing electrical work. Although these basic processes are well understood, a deeper comprehension of the electronic and ionic processes that govern the operation of the DSC is warranted. Transient photocurrent/photovoltage measurements,^{6–12} intensity-modulated photocurrent/photovoltage spectroscopy (IMPS/IMVS),^{6,13–22} and very recently the open circuit voltage decay technique^{23,24} have been used to scrutinize the transport properties of the injected electrons in mesoscopic film and the back reaction with redox species in electrolyte.

Electrochemical impedance spectroscopy (EIS) is a steady-state method measuring the current response to the application of an ac voltage as a function of the frequency.²⁵ An important advantage of EIS over other techniques is the possibility of using tiny ac voltage amplitudes exerting a very small perturbation on the system. EIS has been widely employed to study the kinetics of electrochemical and photoelectrochemical processes including the elucidation of salient electronic and ionic processes occurring in the DSC.^{15,18,26–34} The Nyquist diagram features

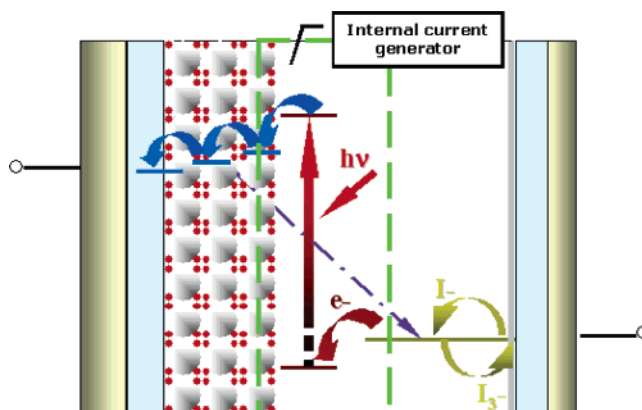


Figure 1. Scheme of a dye-sensitized solar cell.

typically three semicircles that in the order of increasing frequency are attributed to the Nernst diffusion within the electrolyte, the electron transfer at the oxide/electrolyte interface, and the redox reaction at the platinum counter electrode.¹⁵ However, owing to the complexity of the system, the unambiguous assignment of equivalent circuits and the elucidation of processes occurring on dye-sensitized mesoscopic TiO₂ electrode is difficult and remains a topic of current debate.

The present study employs EIS as a diagnostic tool for analyzing in particular photovoltaic performance changes detected during accelerated high-temperature durability tests on dye-sensitized solar cells. A theoretical model is presented interpreting the frequency response in terms of the fundamental electronic and ionic processes occurring in the photovoltaic device. From applying appropriate equivalent circuits, the transport rate and lifetime of the electron in the mesoscopic film are derived and the values are checked by transient photocurrent and photovoltage measurements.

We note that during the final stage of preparation of the present article a paper by Bisquert et al.³⁵ appeared presenting a similar approach to electrochemical impedance investigations of the DSC and that concurs with our analysis.

* To whom correspondence should be addressed. E-mail: michael.gratzel@epfl.ch.

2. Theoretical Modeling of the Frequency Response

The DSC contains three spatially separated interfaces formed by FTO/TiO₂, TiO₂/electrolyte, and electrolyte/Pt–FTO. Electron transfer is coupled to electronic and ionic transport. In the dark under forward bias electrons are injected in the conduction band of the nanoparticles and their motion is coupled to that of I⁻/I₃⁻ ions in electrolyte. Illumination gives rise to new redox processes at the TiO₂/dye/electrolyte interface comprising sensitized electron injection, recombination with the parent dye, and regeneration of the sensitizer. During photovoltaic operation, this “internal current generator” drives all the electronic and ionic processes in the solar cell.³¹ We now derive the equations describing the frequency response of the impedance at the different interfaces.

2.1. I₃⁻ Finite Diffusion within Electrolyte and Electron Transfer at the Pt–FTO/Electrolyte Interface. In practical electrolytes, the concentration of triiodide is much lower than that of iodide and the latter diffuses faster than the former ion. Hence, I⁻ contributes little to the overall diffusion impedance, which is determined by the motion of I₃⁻. The diffusion of I₃⁻ within a thin layer cell is well described by a Nernst diffusion impedance Z_N .^{15,28} Using Fick’s law and appropriate boundary conditions Z_N becomes

$$Z_N = \frac{Z_0}{(i\omega)^\alpha} \tanh(i\tau_d \omega)^\alpha \quad (1)$$

where ω is the angular frequency and α equals 0.5 for a finite length Warburg impedance (FLW). Z_0 and τ_d are the Warburg parameter and characteristic diffusion time constant, respectively, which can be expressed by

$$Z_0 = \frac{RT}{n^2 F^2 c_0 A \sqrt{D}} \quad (2)$$

$$\tau_d = d^2/D \quad (3)$$

where R is the molar gas constant, T the temperature, F the Faraday constant, c_0 the bulk concentration of I₃⁻, A the electrode area, D the diffusion coefficient of I₃⁻, and d is the diffusion length. Because of the mesoporous character of the TiO₂ electrode, a modified Nernst diffusion impedance with α deviating from 0.5 is used to fit the transport of I₃⁻. Nernst diffusion impedance in the Nyquist plot shows typically a straight line at higher frequency along with a semicircle at lower frequency. Fitting Z_0 and τ_d , the diffusion coefficient can be determined.

The charge-transfer resistance R_{CT} associated with the heterogeneous electron exchange involving the I₃⁻ ↔ I⁻ redox couple at the electrolyte/Pt–FTO interface is typically given for the equilibrium potential. From the Butler–Volmer equation, one obtains

$$R_{CT} = \frac{RT}{nF} \frac{1}{i^0} \quad (4)$$

where i^0 is the exchange current density of the reaction. The frequency response of charge-transfer impedance under small sinusoidal perturbation can be expressed as³⁶

$$Z = \frac{iR_{CT}}{i - R_{CT}C_d\omega} \quad (5)$$

where C_d is the double layer capacitance. The charge-transfer

resistance manifests itself as a semicircle in the Nyquist diagram and a peak in the Bode phase angle plot. For electrodes having a rough surface the semicircle is flattened and C_d is replaced by a constant phase element (CPE).

2.2. Electron Transport within the Mesoscopic TiO₂ Film and Electron Loss due to the Reduction of Triiodide at the TiO₂/Electrolyte Interface. When a voltage modulation is applied in the dark to the mesoporous TiO₂ electrode of the DSC, electrons are injected and recovered during the cathodic and anodic parts of the current response. Their collection yield of recollecting the injected electrons depends on their diffusion length

$$L_n = \sqrt{D_e \tau_r} \quad (6)$$

where D_e is the diffusion coefficient and τ_r the lifetime of the electron within the film.

The impedance due to electron diffusion and loss by the interfacial redox reaction in a thin mesoporous layer has been treated by Bisquert.^{31–34} For the case of a mesoscopic TiO₂ film, the diffusion occurs over a finite length and is coupled with interfacial electron-transfer reaction. The electron charge is screened by the electrolyte, which eliminates the internal field, so no drift term appears in the transport equation.⁴ The continuity equation contains therefore only the diffusion and reaction terms.

$$\frac{\partial n}{\partial t} = D_e \frac{\partial^2 n}{\partial x^2} - \frac{(n - n_0)}{\tau_r} \quad (7)$$

the boundary condition being

$$\left. \frac{\partial n}{\partial x} \right|_{x=L} = 0 \quad (8)$$

where n is the concentration of electron, n_0 is their initial concentration, and L is the film thickness. To account for a harmonically modulated voltage, a frequency term is introduced yielding finally for the impedance response:

$$Z = \left(\frac{R_d R_r}{1 + i\omega/\omega_r} \right)^{1/2} \coth[(\omega_r/\omega_d')^{1/2} (1 + i\omega/\omega_r)^{1/2}] \quad (9)$$

where R_d and R_r are the diffusion and dark reaction impedance, respectively, while ω_d' ($\omega_d' = 1/\tau_d' = D_e/L^2$) and ω_r ($\omega_r = 1/\tau_r$) are the corresponding characteristic frequencies. If $R_r \rightarrow \infty$, eq 9 describes a simple diffusion process within restricted boundaries. For a DSC exhibiting a current collection efficiency close to unity, the condition $R_r \gg R_d$ applies and eq 9 becomes

$$Z = \frac{1}{3} R_d + \frac{R_r}{1 + i\omega/\omega_r} \quad (R_r \gg R_d) \quad (10)$$

Under these conditions, the Nyquist plot shows a short straight line at higher frequencies due to diffusion and a large semicircle in the lower frequency regime, indicating fast electron transport and long lifetime of electron in the film. By contrast, if the electron collection efficiency is low, i.e., a major part of the electron reacts with I₃⁻ in the electrolyte before they are recovered at the current collector, the condition $R_d \gg R_r$ applies leading to Gerischer impedance^{34,37}

$$Z = \left(\frac{R_d R_r}{1 + i\omega/\omega_r} \right)^{1/2} \quad (R_d \gg R_r) \quad (11)$$

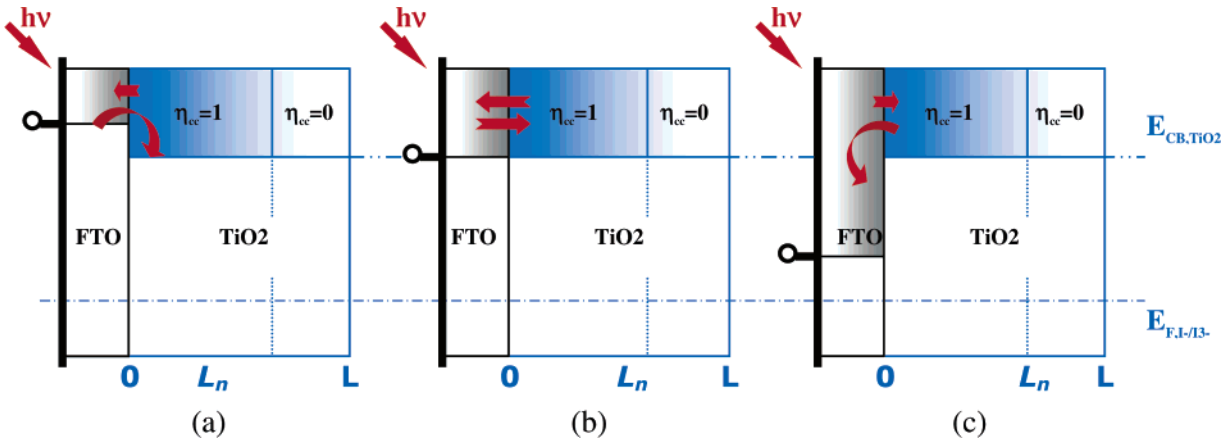


Figure 2. Schematic model of photoanode at different voltages. (a) $E > V_{OC}$; (b) $E = V_{OC}$; (c) $E < V_{OC}$. L is the film thickness, L_n is the electron effective diffusion length, and η_{cc} is the charge collection efficiency of injected electron.

The Gerischer impedance produces response curves similar to a FLW impedance (eq 1). It shows a Warburg diffusion-like straight line at higher frequencies along with a semicircle at lower frequencies. The diffusion coefficient D_e and the lifetime τ_r of the electron in the film can be obtained from eqs 10 and 11.

The above discussion was based on DSC in the dark and under forward bias. Under illumination the continuity equation becomes

$$\frac{\partial n}{\partial t} = \alpha' I \eta_{inj} + D_e \frac{\partial^2 n}{\partial x^2} - \frac{(n - n_0)}{\tau_r} \quad (12)$$

where α' is the effective absorption coefficient, η_{inj} is the quantum yield for charge injection, and I is the incident photon flux, the boundary condition being again given by eq 8.

As indicated in Figure 2, under illumination the short circuit photocurrent J_{SC} of the cell is

$$J_{SC} = J_{inj} - J_{loss} \quad (13)$$

where J_{inj} is the flux of injected electron and J_{loss} is the current from back reaction loss. Since $\eta_{cc} = 1$ for distances $x < L_n$, and $\eta_{cc} = 0$ if $x > L_n$,

$$J_{SC} = J_{inj,x < L_n} - J_{FTO-TiO_2} \quad (14)$$

where $J_{inj,x < L_n}$ is the anodic flux of electron that are injected by the sensitizer and collected at the FTO, while $J_{FTO-TiO_2}$ is the cathodic current flowing from the FTO into the TiO_2 film. Thus,

$$J_{loss} = J_{inj,x > L_n} + J_{FTO-TiO_2} \quad (15)$$

where $J_{inj,x > L_n}$ is the flux of injected electron, which is lost completely before arriving at FTO/ TiO_2 interface. It is clear that $J_{inj,x < L_n} < J_{FTO-TiO_2}$ as $E > V_{OC}$ (Figure 2a); and $J_{inj,x < L_n} > J_{FTO-TiO_2}$ as $E < V_{OC}$ (Figure 2c).

At open circuit state (Figure 2b), $J_{inj,x < L_n}$ equals to $J_{FTO-TiO_2}$, and the total flux is zero. Phenomenologically we can treat the perturbation imposed by the illumination as if a voltage bias was applied in the dark. This applies in particular for a situation where the diffusion length of the electrons is commensurate with or larger than the film thickness. Hence, the same approach as above can be used to analyze its frequency response. Nevertheless, the model may overstate the diffusion rate D_e because photons travel through the film faster than conduction band electrons. But the correction is small if the electron

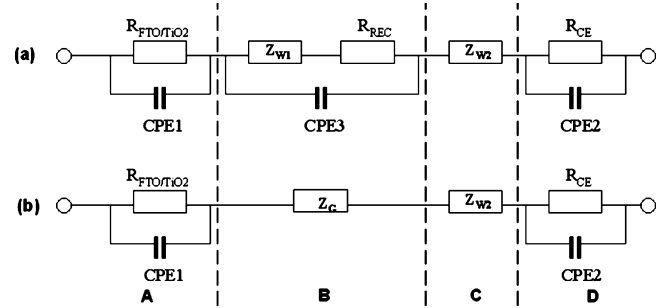


Figure 3. Equivalent circuits of DSC. (a) a cell showing quantitative collection of photoinjected electrons; (b) a cell showing incomplete collection of electrons. Bottom line shows the interpretation of the electrical elements of the equivalent circuit. (A) electron transfer at the FTO/ TiO_2 interface; (B) electron transport and back reaction at the mesoscopic TiO_2 /electrolyte interface; (C) diffusion of I_3^- in the electrolyte; (D) charge transfer at electrolyte/Pt-FTO interface.

diffusion length is long compared to the film thickness L .³¹ Indeed, as will be shown below, in a DSC L_n normally exceeds L rendering this distinction irrelevant.

2.3. Equivalent Circuits and Typical Impedance Spectra of DSC. For a nanoporous electrode, the infinite transmission line is normally used as the equivalent circuit for modeling. For simplicity, only the representative elements displayed in Figure 3 are employed here to model DSC at different states. From left to right, Figure 3 shows the electron transport at the FTO/ TiO_2 interface, electron transport and electron capture by the I_3^- at the TiO_2 /electrolyte interface, diffusion of I_3^- in the electrolyte, and charge transfer at electrolyte/Pt-FTO interface, respectively. For a cell exhibiting a carrier collection efficiency near unity, the condition $R_r \gg R_d$ and eq 10 applies. In this case, the equivalent circuit for the mesoporous TiO_2 film comprises a diffusion element Z_{W1} that is in series connected with the charge-transfer element R_{REC} , the two being in parallel with a capacitive (constant phase angle) element CPE3, as shown in Figure 3a. On the other hand, for cells where only a fraction of the photogenerated charge carriers are collected, the condition of $R_d \gg R_r$ applies and a single Gerischer impedance element Z_G describes the diffusion of the electron in the mesoscopic TiO_2 film and their recapture by the triiodide ions in the electrolyte (Figure 3b). R_{FTO/TiO_2} is the resistance of the FTO/ TiO_2 contact and CPE1 is the capacitance of this interface. The latter feature, due to overlap with other processes, is not easily distinguished. Z_{W2} is the Warburg impedance describing the diffusion of I_3^- in the electrolyte, R_{CE} is the charge-transfer

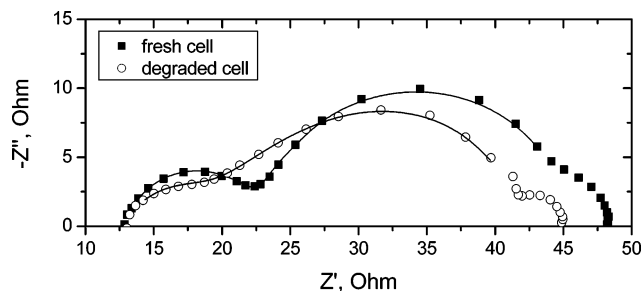


Figure 4. Typical Nyquist plots of a N719 sensitized DSC. Filled squares, fresh cell; open circles, cell after aging for 48 h at 80 °C. The lines show theoretical fits using the equivalent circuits shown in Figure 3a and b, respectively. The electrolyte is 0.6 M PMII, 0.1 M I₂, and 0.5 M NMB in MPN.

impedance at the counter electrode, and CPE2 is the double layer capacitance at the electrolyte/Pt–FTO interface.

A typical EIS spectrum for a DSC exhibits three semicircles in the Nyquist plot or three characteristic frequency peaks in a Bode phase plot. This is illustrated in Figure 4 showing Nyquist plots of a N719 sensitized DSC before and after thermal aging at 80 °C for 2 days. The response in the intermediate-frequency regime changes greatly upon aging, indicating the conversion of a Nernst to a Gerischer impedance. Apparently, the spectra can be well fitted in terms of the corresponding equivalent circuits in Figure 3. These models will therefore be employed to interpret impedance data in the following sections.

3. Experimental Section

3.1. Dye-Sensitized Mesoscopic TiO₂ Electrode Preparation and Cell Fabrication. The preparation of mesoscopic TiO₂ film has been described in ref 38. The screen-printed double-layer film consists of a 10- μ m transparent layer and a 4- μ m scattering layer whose thickness was determined by using an Alpha-step 200 surface profilometer (Tencor Instruments). A porosity of 0.63 for the transparent layer was measured with a Gemini 2327 nitrogen adsorption apparatus (Micromeritics Instrument Corp.). The film was heated to 500 °C in air and calcinated for 20 min before use. Then the still hot spots were dipped into a 2 \times 10⁻⁴ M 2-fold deprotonated cis-RuL2(SCN)2

(L = 2,2'-bipyridyl-4,4'-dicarboxylic acid) (N719) or cis-RuLL'-(SCN)₂ (L = 2,2'-bipyridyl-4,4'-dicarboxylic acid, L' = 4,4'-dinonyl-2,2'-bipyridyl) (Z907) dye (Chart 1) solution in acetonitrile/*tert*-butyl alcohol (1:1) and left for overnight. Finally, the dye-coated electrodes were rinsed with acetonitrile. For transient photocurrent/photovoltage measurements, single transparent TiO₂ films with the thickness of 12 μ m were used.

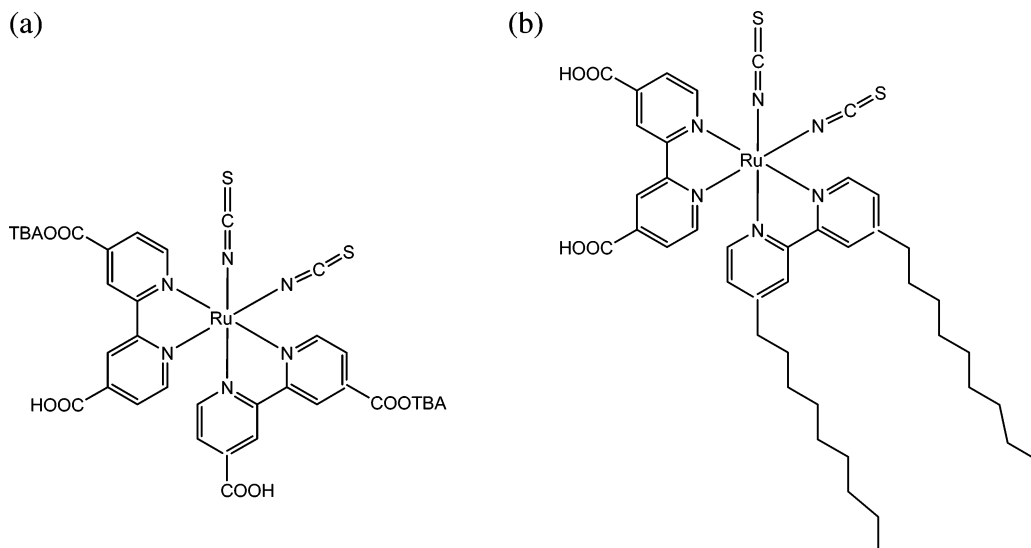
A sandwich cell was prepared using the dye-sensitized electrode as the working electrode and a platinum-coated conducting glass electrode as the counter electrode. The latter was prepared by chemical deposition of platinum from 0.05 M hexachloroplatinic acid at 400 °C. The two electrodes were placed on top of each other using a thin transparent film of Bynel polymer (DuPont) as a spacer. The empty cell was tightly held, and the edges were heated to 130 °C in order to seal the two electrodes together. A thin layer of electrolyte was introduced into the interelectrode space from the counter electrode side through a predrilled hole. The hole was sealed with a microscope cover slide and Bynel to avoid leakage of the electrolyte solution. There were two electrolytes used in this paper: electrolyte 1, 0.6 M PMII, 0.1 M I₂, and 0.5 M NMB in MPN; electrolyte 2, 0.6 M DMPPII, 0.05 M I₂, 0.5 M tBuPy, 0.1 M LiI in AN:VN(1:1). Thermal stress tests were carried out by putting cells in an oven at 80 °C and then measuring the *I*–*V* curve, impedance and transient photocurrent/photovoltage.

3.2. *I*–*V* Measurements. A 450-W xenon light source (Osram XBO 450) was used as the irradiation source for the *I*–*V* measurements. The spectral output of the lamp matched the AM 1.5 solar spectrum in the region of 350–750 nm (mismatch <2%). Incident light intensities were adjusted with neutral wire mesh attenuators. The current–voltage characteristics were determined by applying an external potential bias to the cell and measuring the photocurrent using a Keithley model 2400 digital source meter (Keithley). The overall conversion efficiency η of the photovoltaic cell is calculated from the integral photocurrent density (*J*_{SC}), the open-circuit photovoltage (*V*_{OC}), the fill factor of the cell (*ff*), and the intensity of the incident light (*I*_{Ph}),

$$\eta = J_{SC} \cdot V_{OC} \cdot ff / I_{Ph} \quad (16)$$

3.3. Electrochemical Impedance Measurements. Impedance measurements were performed with a computer-controlled

CHART 1: Sensitizers Used in This Study^a



^a Key: (a) N719; (b) Z907.

potentiostat (EG&G, M273) equipped with a frequency response analyzer (EG&G, M1025). The frequency range is 0.005–100 kHz. The magnitude of the alternative signal is 10 mV. Unless otherwise mentioned, all impedance measurements were carried out under a bias illumination of 100 mW/cm² (global AM 1.5, 1 sun) from a 450-W xenon light source. The obtained spectra were fitted with Z-View software (v2.1b, Scribner Associate, Inc.) in terms of appropriate equivalent circuits.

3.4. Transient Photocurrent/Photovoltage Measurements.

Transient photocurrent and photovoltage studies of the DSC were carried out by using weak laser pulses at $\lambda = 514$ nm, superimposed on a relatively intense bias illumination. The bias light was supplied by a cw 450-W Xe arc lamp, equipped with a water filter and a 680-nm cutoff filter. The continuous wave beam was condensed by a lens to irradiate a ~ 1 cm² cross section of the cell, the surface of which was kept at a 60° angle to the beam. The red light intensity measured at the cell position was typically 120 mW/cm². The cell was oriented to expose the counter electrode side to both the bias light and laser beams. The 5-ns-duration laser pulses at a wavelength of 514 nm were generated by a broadband optical parametric oscillator (GWU, OPO-355) pumped by the third harmonic of a 30-Hz repetition rate, Q-switched Nd:YAG laser (Continuum, Powerlite 7030). The laser beam was attenuated by gray filters to restrict the pulse fluence onto the cell to < 100 μ J/cm². The 514-nm laser light was strongly absorbed by the dye, and therefore, injected electrons were introduced into a narrow spatial region, corresponding to where the probe light enters the film. Current transients were measured across a 20 Ω resistor load using a large bandwidth digital signal analyzer (Tektronix DSA 602A). Transient photovoltages were measured by feeding the signal directly into the DSA amplifier, whose impedance was 1 M Ω .

4. Results and Discussion

4.1. Impedances of DSC Obtained in Dark and Illumination. There are different processes that occur in the cell in the dark or under illumination. At open circuit voltage and in sunlight, there is no net current flowing through the cell. All the injected electrons are recaptured by I₃⁻ before being extracted to the external circuit. Meanwhile, the oxidized dye is regenerated by I⁻. As a result, the absorbed photon energy is converted to heat through the two coupled redox cycles involving sensitized electron injection, dye regeneration, and electron recapture by I₃⁻. The counter electrode is kept at equilibrium, because there is no net current flowing through it. However, in the dark under forward bias, electrons are transported through the mesoscopic TiO₂ network and react with I₃⁻. At the same time, I⁻ is oxidized to I₃⁻ at the counter electrode. The net current density can be large depending on the applied bias voltage.

Figure 5 shows the impedance spectra of a DSC measured at OCV (-0.68V) under 1 sun and under forward bias (-0.68 V) in the dark. Strikingly, the impedance due to electron transfer from the conduction band of the mesoscopic film to triiodide ions in the electrolyte, presented by the semicircle in intermediate-frequency regime, is much smaller under light than in the dark even though the potential of the film is the same. Correspondingly, the characteristic frequency shown in Bode phase plots increases two times, suggesting the electron lifetime is shortened by a factor of 2. This can be ascribed to a difference in the local I₃⁻ concentration. Under illumination, I₃⁻ is formed "in situ" by dye regeneration at the mesoporous TiO₂/electrolyte interface, whereas in the dark, I₃⁻ is generated at counter

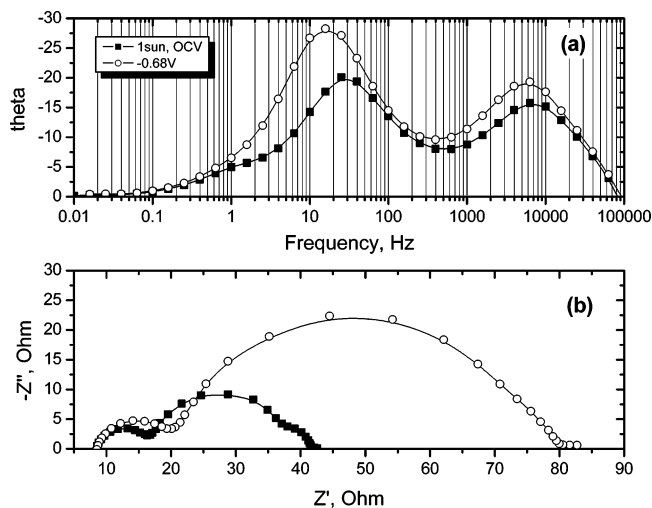


Figure 5. Impedance spectra of a Z907 cell measured at OCV (-0.68 V), 1 sun or at -0.68 V in dark. (a) Bode phase plots; (b) Nyquist plots. Electrolyte 1 is used.

electrode and penetrates the mesoporous TiO₂ films by diffusion. As indicated by eq 17, the higher local I₃⁻ concentration produced in the porous network under light is expected to accelerate the recapture of conduction band electrons and shortens their lifetime within the TiO₂ film.

$$J_r = ek_r c_{\text{ox}}^\gamma (n^\beta - n_0^\beta) \quad (17)$$

Here J_r is the I₃⁻ reduction current, k_r is the rate constant of the reduction reaction, and c_{ox} is the concentration of I₃⁻; the exponents γ and β are the reaction orders for I₃⁻ and electrons, respectively.

4.2. Impedance of DSC with Different Electrolytes.

Electrolytes exert a great influence on the photovoltaic performance of the DSC by effecting the kinetics of electronic or ionic processes. For instance, acetonitrile (AN)-based electrolytes have much lower viscosity compared with 3-methoxypropionitrile (MPN), the kinetics of dye regeneration, I₃⁻ \rightarrow I⁻ reaction at counter electrode, electron transport within the TiO₂ film, and I⁻/I₃⁻ diffusion in electrolyte being faster in the former case. Consequently, much better photovoltaic performance has been achieved. In addition, additives in the electrolyte are of great importance for optimization and stabilization of the TiO₂/dye/electrolyte interface. TBP,³⁹ NMB,⁴⁰ and recently guanidinium salts⁵ have been shown to be effective in increasing the photovoltage without greatly reducing the photocurrent.

Figure 6 shows the impedance spectra of a Z907 sensitized cell with two kinds of electrolytes at different light intensity. From the Bode phase plots, the electron lifetime with electrolyte 2 is much longer than that obtained with electrolyte 1 at the same light intensity. According to Frank et al., it is believed that Li⁺ in electrolyte 2 plays an important role for the long lifetime of the electron.¹¹ The characteristic time constants of electron transport and back reaction are obtained by fitting the spectra with the equivalent circuit shown in Figure 3a. The electron diffusion rate D_e of the cell with electrolyte 2 is 2×10^{-4} cm²/s at 1 sun, 3 times higher than that obtained from IMPS by Peter et al. in an AN-based electrolytes.^{16,22} That of electrolyte 1 is 1.1×10^{-4} cm²/s, close to the value obtained from photocurrent transient measurements.¹² From eq 18, the effective diffusion length L_n of the conduction band electrons is calculated to be ~ 16.2 μ m for MPN-based electrolyte 1 at 1 sun and at open circuit voltage. That of electrolyte 2 is ~ 30.1

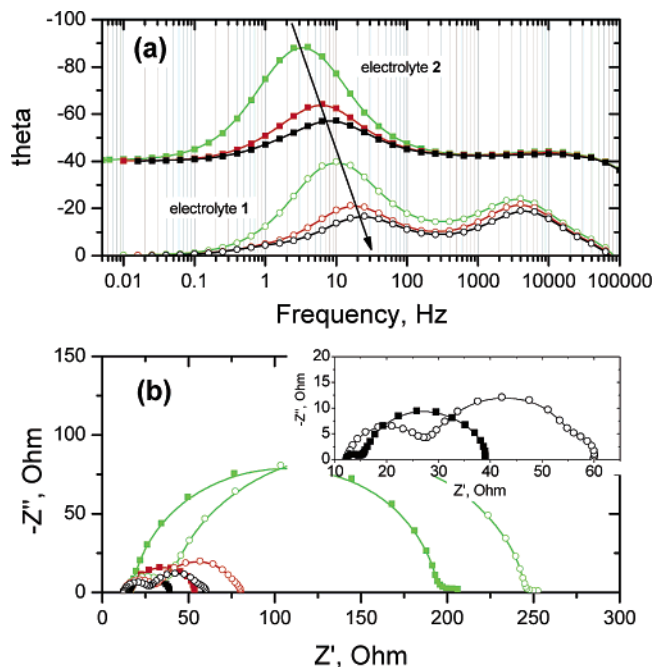


Figure 6. Impedance spectra of Z907 cells at different light intensity, 0.1 sun (green), 0.5 sun (red), and 1 sun (black). (a) Bode phase plots; (b) Nyquist plots. Electrolyte 1, open circles; electrolyte 2, filled squares. The inset of (b) shows the spectra at 1 sun for both electrolytes.

μm . The latter being much larger than the film thickness, all photogenerated electrons will be collected.

$$L_n = L\sqrt{\frac{\tau_r}{\tau_d'}} = L\sqrt{\frac{\omega_d'}{\omega_r}} \quad (18)$$

In addition, the charge-transfer impedance at the counter electrode with electrolyte 2 is much smaller than that of electrolyte 1, which is in accordance with the lower exchange current density for the iodide/triiodide couple in the latter electrolyte.

A light intensity effect on the electron lifetime is apparent in both electrolytes. Under illumination, V_{OC} can be expressed as⁴¹

$$V_{OC} = \frac{RT}{\beta F} \ln\left(\frac{AI}{n_0k_1[I_3^-] + n_0k_2[D^+]}\right) \quad (19)$$

with k_1 and k_2 being, respectively, the kinetic constant of back reaction of injected electrons with triiodide and recombination of these electrons with oxidized dye and n_0 being the concentration of accessible electronic states in the conduction band. Neglecting the loss term due to recombination with the oxidized dye molecules, V_{OC} depends logarithmically on the inverse concentration of I_3^- and increases with incident photon flux I . The V_{OC} of the cell with electrolyte 2 are 0.614, 0.665, and 0.681 V at 0.1, 0.5 and 1 sun, respectively. Those with electrolyte 1 are 0.651, 0.707, and 0.725 V, respectively, following the predicted logarithmical relation. Any variations of the local triiodide concentration due to light illumination appear to have a small effect.

For comparison, transient photocurrent/photovoltage measurements were also performed. Figure 7a shows the transient photocurrent curves of Z907 cell with two electrolytes at short circuit state, presenting a multicomponent process. The characteristic time constant τ_c can be fitted to one major single-exponential decay process, where the diffusion coefficient D_e

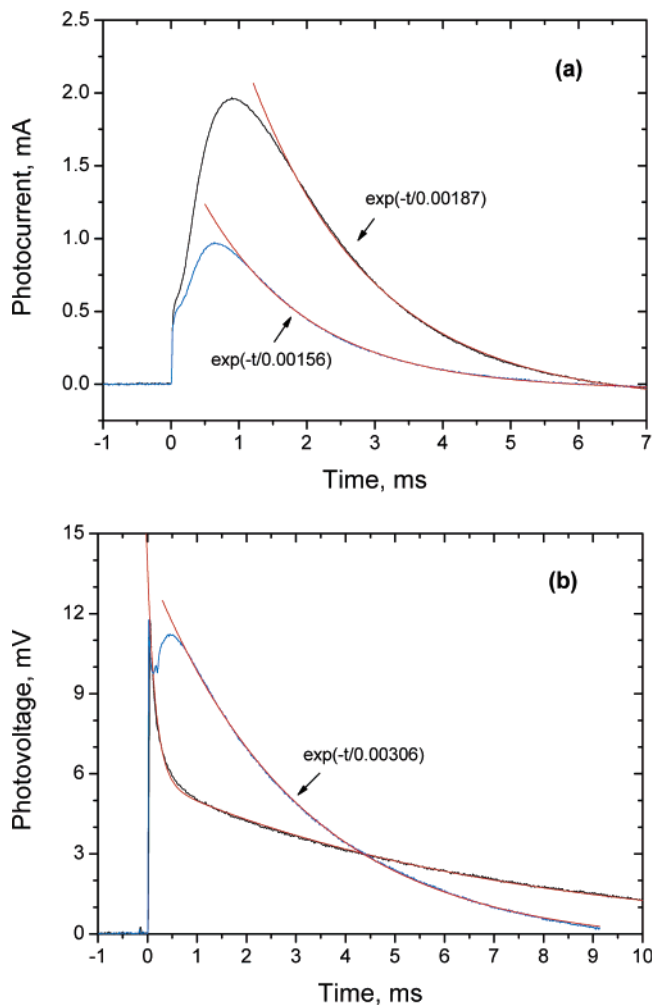


Figure 7. Transient photocurrent (a) and photovoltage (b) of Z907 cells with electrolyte 1 (blue line) and 2 (black line). The red lines are the corresponding computer fits for the decay processes. The inset equations show time constants for the exponential decay.

is estimated from eq 20.⁸ The fitted τ_c values are 1.56 and 1.87 ms, and for a 12- μm -thick film, the calculated D_e are 3.9×10^{-4} and $3.3 \times 10^{-4} \text{ cm}^2/\text{s}$ for electrolytes 1 and 2, respectively. These electron diffusion coefficients are higher than those obtained from the EIS measurement. This is probably due to the fact that the bias light intensity used for these measurements was larger than 1 sun, giving a higher electron concentration within the film and consequently a faster electron diffusion rate.⁹ Also, because the fast back reaction accelerates the decay process, the value for the MPN-based electrolyte obtained from transient photocurrent measurement is overstated (J_{SC} for electrolyte 2 is 12.3 mA/cm^2 , whereas that of electrolyte 1 is only 7.9 mA/cm^2).

$$D_e = L^2/(2.35\tau_c) \quad (20)$$

Figure 7b shows the transient photovoltage curves of the same cells at open circuit. The fitted time constant τ_R for electrolyte 1 is ~ 3.1 ms, whereas because of the large capacitive current, τ_R cannot be obtained for the cell with the AN-based electrolyte. The lifetime obtained from transient photovoltage measurement is again shorter than that from the EIS measurement for the same reasons that have been given above. After correcting the capacitive charging effects, electrolyte 2 has a longer lifetime than electrolyte 1 in agreement with the EIS measurements.

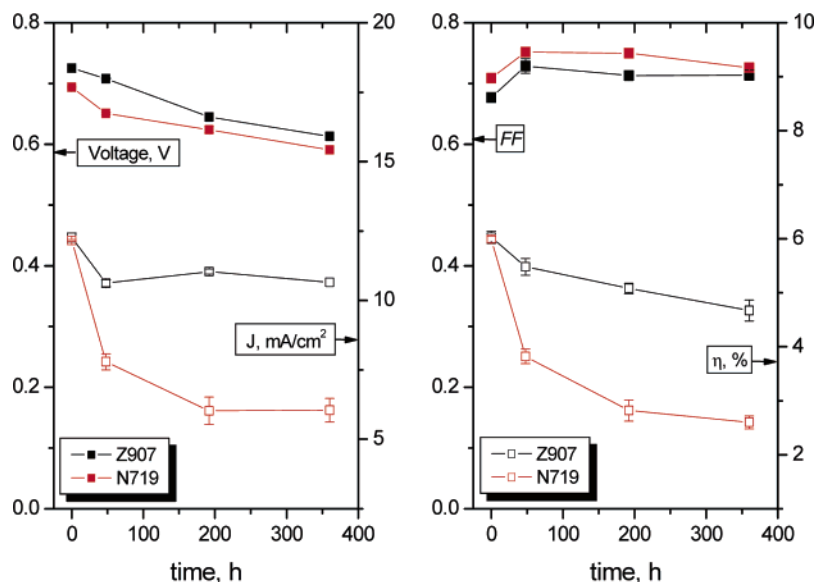


Figure 8. Photovoltaic performances of N719 and Z907 cells during continuous thermal stress at 80 °C. Electrolyte 1 was used for both cells. The data were obtained from the average of two cells for each dye.

4.3. Evolution of the DSC under Thermal Stress. Achieving stable performance under a high-temperature accelerated aging test is important for outdoor DSC applications. Even though devices with efficiency retention of over 90% after 1000 h of thermal stress at 80 °C have been realized by careful selection of dye molecules and electrolytes,⁴⁰ keeping the TiO₂/dye/electrolyte interface stable during prolonged thermal stress is still a challenging task especially if the V_{OC} is to remain completely constant under these adverse conditions of accelerated thermal testing.⁴² Impedance measurements provide a powerful tool to analyze this behavior, offering clues to remedy any unwanted photovoltaic performance changes. In this section, the impedance spectra of DSCs with two kinds of sensitizers during continuous thermal stress are studied, and the results are linked to the evolution of the electron lifetime, electron transport rate, and charge transfer at the counter electrode.

As shown in Figure 8, the photovoltaic performance of the Z907 sensitized cell is much more stable than that of the N719 cell. After 360 h of thermal stress, the efficiency retention for this particular sensitizer/electrolyte combination was close to 85%, whereas it was less than 50% for the N719 cell. The performance decline of the N719 cell results mainly from the large drop of photocurrent especially at the beginning of thermal aging. In addition, a slow decline in photovoltage is apparent for both cells.

Figure 9 presents the impedance spectra of the two cells at different aging times. It is clear from Bode phase plots that the electron lifetimes for both cells decrease significantly during thermal stress. However, from the characteristic frequency, that of the Z907 cell remains always much longer than that of the N719 device. It is interesting that the charge-transfer impedance at the counter electrode after 2 days of thermal aging decreases for both cells, consistent with the improvement of the fill factor over the same period. This is attributed to the activation or better contact between electrolyte and Pt catalyst. For both sensitizers, the impedance spectra of a fresh cell can be well fitted with the equivalent circuit in Figure 3a. After thermal aging, the spectrum of the Z907 cell still reflects this equivalent circuit, whereas that of the N719 cell can only be fitted using a Gerischer impedance as suggested in Figure 4. According to eq 11, the diffusion impedance becomes larger than that of the back reaction, leading to incomplete charge carrier collection due to

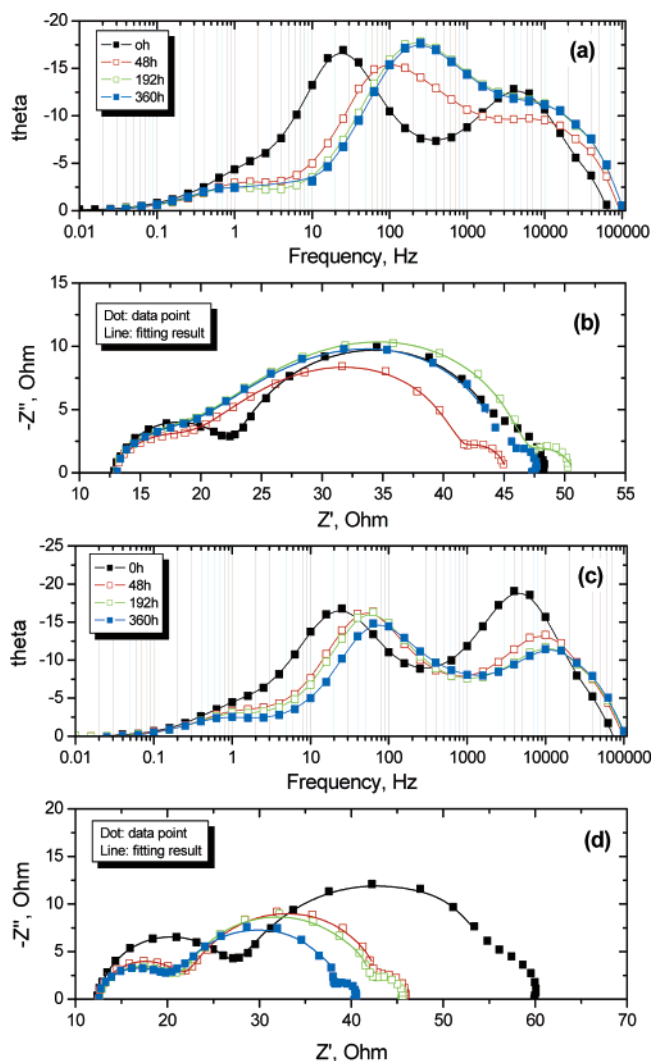


Figure 9. Impedance spectra of N719 (a), (b) and Z907 (c), (d) cells in Figure 8 during continuous thermal aging at 80 °C. The lines in (b) and (d) show the fitted results.

the reduction of the effective electron diffusion length. This is responsible for the large drop of the photocurrent during thermal aging.

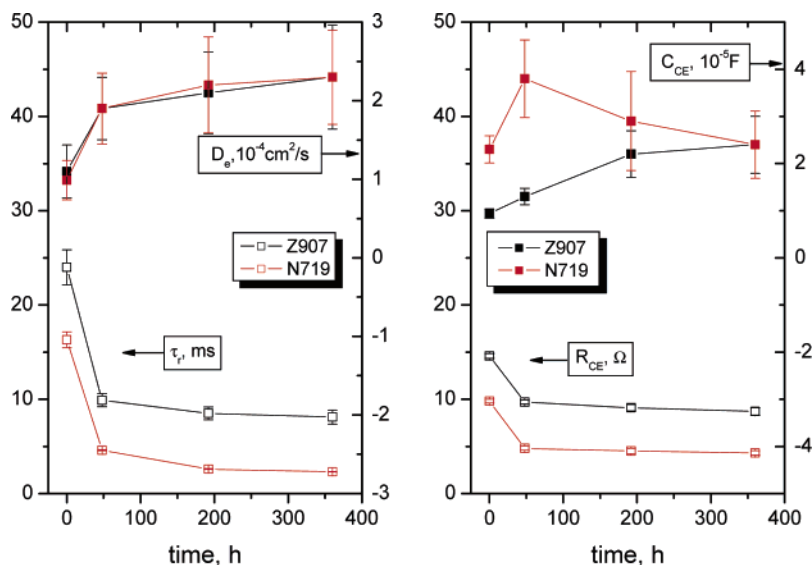


Figure 10. Evolution of kinetic and electrical cell parameters from fitting the spectra in Figure 9 during continuous thermal stress of N719 and Z907 cells at 80 °C.

The fitted parameters are presented in Figure 10. The electron diffusion rates D_e are in the order of 10^{-4} cm²/s for both sensitizers. Thermal stress gives rise to an increase of the diffusion rate but, at the same time, a significant decrease of the electron lifetime τ_r . The values of τ_r are around 24 and 16 ms for the fresh Z907 and N719 cells, respectively. They decrease 2–3 times after 2 days of thermal aging. That of the N719 cell attains values below 5 ms, making the electron diffusion length shorter than the film thickness.

Because both dye molecules are stable during thermal stress, it is concluded from the impedance measurements that the TiO₂/dye/electrolyte interface is much more stable for Z907 cell. Desorption of the dye at the elevated temperature could play a role, and this is supported by the fact that the observed performance changes are at least partially reversible. In particular, almost complete performance recovery can be observed when the thermally aged cells are subjected to illumination at 60 °C. The reasons for this complex behavior remain to be explored. The hydrophobic chain of Z907 dye may prevent interfering impurity species in particular water from accumulating at the interface, explaining the stability. By contrast, the N719 derivatized TiO₂ surface is more prone to intrusion of water and other things during prolonged thermal aging, which may enhance the rate of recapture of the injected electrons by the triiodide ions in the electrolyte.

5. Conclusions

Electrochemical impedance spectroscopy is a powerful steady-state technique to study dye-sensitized solar cells. Under open circuit condition, key parameters characterizing electron transport, back reaction, charge transfer at a counter electrode, etc., can be extracted by applying appropriate equivalent circuits. These parameters predict well the photovoltaic performance of the cells in agreement with the transient techniques. The latter are less suited to interpret cell aging phenomena due to the interference by charge recombination. Also, EIS is not perturbed by the capacitive charging currents that hamper time-resolved photocurrent and photovoltage measurements. The present analysis shows that EIS is very useful to unravel the reasons for photovoltaic performance changes during aging experiments, offering valuable clues for avoiding these unwanted phenomena.

Acknowledgment. We acknowledge financial support of this work by the Swiss Federal Office for Energy (OFEN) and the Swiss National Science Foundation. We thank Dr. Shaik M. Zakeeruddin and Md. K. Nazeeruddin for providing the sensitizers and Mr. P. Comte and R. Charvet for the mesoscopic TiO₂ films.

References and Notes

- O'Regan, B.; Grätzel, M. *Nature* **1991**, *353*, 737.
- Grätzel, M. *Nature* **2001**, *414*, 338.
- Nazeeruddin, M. K.; Kay, A.; Rodicio, I.; Humphry-Baker, R.; Müller, E.; Liska, P.; Vlachopoulos, N.; Grätzel, M. *J. Am. Chem. Soc.* **1993**, *115*, 6382.
- Hagfeldt, A.; Grätzel, M. *Chem. Rev.* **1995**, *95*, 49.
- Grätzel, M. *J. Photochem. Photobiol. A* **2004**, *164*, 3.
- Nakade, S.; Saito, Y.; Kubo, W.; Kitamura, T.; Wada, Y.; Yanagida, S. *J. Phys. Chem. B* **2003**, *107*, 8607.
- Peter, L. M.; Ponomarev, E. A.; Franco, G.; Shaw, N. J. *Electrochim. Acta* **1999**, *45*, 549.
- van de Lagemaat, J.; Frank, A. J. *J. Phys. Chem. B* **2001**, *105*, 11194.
- Kopidakis, N.; Schiff, E. A.; Park, N. G.; van de Lagemaat, J.; Frank, A. J. *J. Phys. Chem. B* **2000**, *104*, 3930.
- O'Regan, B. C.; Lenzmann, F. *J. Phys. Chem. B* **2004**, *108*, 4342.
- Kopidakis, N.; Benkstein, K. D.; van de Lagemaat, J.; Frank, A. J. *J. Phys. Chem. B* **2003**, *107*, 11307.
- Benkstein, K. D.; Kopidakis, N.; van de Lagemaat, J.; Frank, A. J. *J. Phys. Chem. B* **2003**, *107*, 7759.
- Oekermann, T.; Yoshida, T.; Minoura, H.; Wijayantha, K. G. U.; Peter, L. M. *J. Phys. Chem. B* **2004**, *108*, 8364.
- Bisquert, J.; Vkhrenko, V. S. *J. Phys. Chem. B* **2004**, *108*, 2313.
- Kern, R.; Sastrawan, R.; Ferber, J.; Stangl, R.; Luther, J. *Electrochim. Acta* **2002**, *47*, 4213.
- Fisher, A. C.; Peter, L. M.; Ponomarev, E. A.; Walker, A. B.; Wijayantha, K. G. U. *J. Phys. Chem. B* **2000**, *104*, 949.
- Peter, L. M.; Wijayantha, K. G. U. *Electrochim. Acta* **2000**, *45*, 4543.
- van de Lagemaat, J.; Park, N. G.; Frank, A. J. *J. Phys. Chem. B* **2000**, *104*, 2044.
- Franco, G.; Gehring, J.; Peter, L. M.; Ponomarev, E. A.; Uhlendorf, I. *J. Phys. Chem. B* **1999**, *103*, 692.
- Schlichthörl, G.; Park, N. G.; Frank, A. J. *J. Phys. Chem. B* **1999**, *103*, 782.
- Schlichthörl, G.; Huang, S. Y.; Sprague, J.; Frank, A. J. *J. Phys. Chem. B* **1997**, *101*, 8141.
- Dloczik, L.; Ieperuma, O.; Lauermann, I.; Peter, L. M.; Ponomarev, E. A.; Redmond, G.; Shaw, N. J.; Uhlendorf, I. *J. Phys. Chem. B* **1997**, *101*, 10281.

- (23) Bisquert, J.; Zaban, A.; Greenshtein, M.; Mora-Sero, I. *J. Am. Chem. Soc.* **2004**, *126*, 13550.
- (24) Zaban, A.; Greenshtein, M.; Bisquert, J. *ChemPhysChem* **2003**, *4*, 859.
- (25) Ross, M. J.; William, K. R. *Impedance Spectroscopy: Emphasizing Solid Materials and Systems*; John Wiley & Sons: New York, 1987.
- (26) Bisquert, J. *Phys. Chem. Chem. Phys.* **2003**, *5*, 5360.
- (27) Han, L. Y.; Koide, N.; Chiba, Y.; Mitate, T. *Appl. Phys. Lett.* **2004**, *84*, 2433.
- (28) Hauch, A.; Georg, A. *Electrochim. Acta* **2001**, *46*, 3457.
- (29) Zaban, A.; Meier, A.; Gregg, B. A. *J. Phys. Chem. B* **1997**, *101*, 7985.
- (30) Schwarzburg, K.; Willig, F. *J. Phys. Chem. B* **2003**, *107*, 3552.
- (31) Pitarch, A.; Garcia-Belmonte, G.; Mora-Sero, I.; Bisquert, J. *Phys. Chem. Chem. Phys.* **2004**, *6*, 2983.
- (32) Bisquert, J. *Phys. Chem. Chem. Phys.* **2000**, *2*, 4185.
- (33) Bisquert, J.; Garcia-Belmonte, G.; Fabregat-Santiago, F.; Ferriols, N. S.; Bogdanoff, P.; Pereira, E. C. *J. Phys. Chem. B* **2000**, *104*, 2287.
- (34) Bisquert, J. *J. Phys. Chem. B* **2002**, *106*, 325.
- (35) Fabregat-Santiago, F.; Bisquert, J.; Garcia-Belmonte, G.; Boschloo, G.; Hagfeldt, A. *Sol. Energy Mater. Sol. Cells* **2005**, *87*, 117.
- (36) Bard, A. J.; Faulkner, L. R. *Electrochemical Methods: Fundamentals and Applications*, 2nd ed.; John Wiley & Sons: New York, 2000.
- (37) Boukamp, B. A.; Bouwmeester, H. J. M. *Solid State Ionics* **2003**, *157*, 29.
- (38) Barbé, C. J.; Arendse, F.; Comte, P.; Jirousek, M.; Lenzmann, F.; Shklover, V.; Grätzel, M. *J. Am. Ceram. Soc.* **1997**, *80*, 3157.
- (39) Huang, S. Y.; Schlichthorl, G.; Nozik, A. J.; Grätzel, M.; Frank, A. J. *J. Phys. Chem. B* **1997**, *101*, 2576.
- (40) Wang, P.; Zakeeruddin, S. M.; Moser, J. E.; Nazeeruddin, M. K.; Sekiguchi, T.; Grätzel, M. *Nat. Mater.* **2003**, *2*, 402.
- (41) Koelsch, M.; Cassaignon, S.; Thanh Minh, C.Ta; Guillemoles, J.-F.; Jolivet, J.-P. *Thin Solid Films* **2004**, *451–452*, 86.
- (42) Wang, P.; Klein, C.; Humphry-Baker, R.; Zakeeruddin, S. M.; Grätzel, M. *Appl. Phys. Lett.* **2005**, *86*, 123508.